Chapter 10

Constraining the inner regions of protostellar envelopes through mid-infrared observations

Abstract

This chapter briefly discusses the perspectives of using mid-infrared observations to constrain the physical properties of the inner envelopes of low-mass protostars and their ice content. Through observations with, e.g., the Spitzer Space Telescope and infrared cameras on 8 m class telescopes, the inner radius of the envelopes, as well as the spectral energy distribution (SED) of the central heating source (possibly also reflecting the presence of any circumstellar disk), can be constrained in cases where the envelopes are relatively optically thin. This provides a strong additional constraint on the envelope structure, although it does not affect the interpretation of the far-infrared and (sub)millimeter SEDs and images presented in previous chapters.

Parts of the results discussed in this chapter have been presented in two papers in the ApJS, 2004, Spitzer issue (Young, Jørgensen, Shirley et al. and Boogert, Pontoppidan, Lahuis, Jørgensen et al.). A future paper (Jørgensen et al. in prep.) will present the results discussed in this chapter in more details.

10.1 Introduction

The physical conditions in the envelopes around young stellar objects are of great importance for models of protostellar collapse and their subsequent early evolution, and for interpreting the molecular excitation to constrain the chemistry. Although the models derived on basis of the far-infrared through millimeter SEDs and continuum images (Chapter 2, Schöier et al. 2002; Shirley et al. 2002) work well to describe the physical structure down to 500 AU scales (Chapter 5, 6 and 7), the dust content of the innermost regions where the temperatures increase to $\gtrsim$100 K remains elusive through such observations and one has to rely on extrapolations from the properties of the outer envelopes. Interesting questions therefore remain unanswered: is there an inner cavity of the envelopes, e.g., established through the angular momentum barrier (e.g., Terebey et al. 1984)? What are the more precise properties of the central newly formed protostar and of the circumstellar disk? Is it for example possible to constrain their spectral energy distributions in greater detail (as discussed in Chapter 5)? Do the dust opacities change with temperature and radius throughout the envelopes, e.g., from grains with ice mantles in the outer regions to grains without in the innermost regions? So where do we go from

here in order to address these questions?

Interesting additional constraints on the physical structure of the warm dust in the inner envelopes can come from deep mid-infrared observations using the cameras and spectrographs on the Spitzer Space Telescope and on 8 m class telescopes including the VLT, Keck, Subaru and Gemini. Also, since so much of the chemistry in these protostellar envelopes is dominated by freeze-out (e.g., Chapters 2, 3, 4 and 6) it is an interesting task to start using the models established so-far to address the detailed ice composition self-consistently for comparison to the near- and mid-infrared observations by, e.g., Boogert et al. (2002) and Pontoppidan et al. (2003). This chapter briefly discusses some of the early results from modeling of mid-infrared observations obtained within the Spitzer Space Telescope, "Cores to Disks" (c2d) legacy program (Evans et al. 2003). Parts of the results discussed in this chapter have been presented in two papers in the ApJS, 2004, "Spitzer issue" (Young, Jørgensen, Shirley et al. and Boogert, Pontoppidan, Lahuis, Jørgensen et al.). A future paper (Jørgensen et al. in prep.) will present the results discussed in this chapter in more elaborate details.

10.2 Sources and observations

The basis for this discussion is formed by the submillimeter, far- and mid-infrared observations of three pre- and protostellar objects L1014, B5-IRS1 and HH46-IRS, which were observed during the validation period of Spitzer for the c2d legacy program. Only a short overview of the sources and observations is given here.

B5-IRS1 (IRAS 03445+3242) is the most "simple" of the three sources, a typical young stellar object in Perseus (at 220 pc) with a well-studied wide-angle outflow (e.g. Velusamy & Langer 1998). It was observed with the *IRS* spectrograph on Spitzer (Boogert et al. 2004) with resolution, $\lambda/\Delta\lambda$, of $\approx$ 60–600. Combined with ground-based observations from NIRSPEC on Keck this provides its full SED in the range from 2 to 34 μm. B5-IRS1 has furthermore been observed by IRAS (60 and 100 μm), SCUBA (archival data) and at 1.3 mm by Motte & André (2001).

L1014 is a dark, relatively compact, "Lynds" cloud (Lynds 1962) with no known IRAS source (e.g., Visser et al. 2002) at a distance of about 200 pc. It was observed in the "Core" part of the c2d program using the two infrared cameras on Spitzer, IRAC and MIPS, at 3.6, 4.5, 6.0 and 8.0 μm (IRAC) and 24 and 70 μm (MIPS). Complementary data were obtained from a number of facilities including continuum maps from the SCUBA archive and MAMBO on the IRAM 30 m. Given its tentative classification as a pre-stellar core it was rather surprising that an infrared source, L1014-IRS, was in fact observed by both IRAC and MIPS.

HH46-IRS (IRAS 08242-5050) is a deeply embedded southern source at 460 pc. Infrared images from the IRAC and MIPS cameras show emission from the prominent outflow (e.g. Heathcote et al. 1996; Noriega-Crespo et al. 2004).

Like B5-IRS1 it was observed with Spitzer/IRS, and the data were combined with ground-based observations from ISAAC on the VLT. It was observed with ISO-LWS between 45 and 180 μm, and with JCMT/SCUBA at 850 μm despite its location far south at low elevation ($\approx 25^{\circ}$) (Correia et al. 1998).

For all three sources SCUBA data were obtained from the archive and re-reduced for this discussion. For further details about the mid-infrared observations we refer to the papers by Boogert et al. (2004) and Young et al. (2004).

10.3 Models

B5-IRS1

The first example in this discussion is the B5-IRS1 protostar: as in Jørgensen et al. (2002, 2004b), the envelope properties were constrained through 1D radiative transfer assuming a spherically symmetric envelope with a power-law density profile ($n \propto r^{-p}$), heated by a central blackbody. The submillimeter emission constrains the envelope density profile and, to some degree, the outer radius of the envelope. However, the inner radius and spectral energy distribution of the central heating source are not well-determined through the submillimeter data: for the models presented in the previous chapters an inner temperature of 250 K and a central blackbody of 5000 K were assumed.

The mid-infrared observations, however, provide interesting complementary constraints on the envelope properties as illustrated in Fig. 10.1–10.2 for B5-IRS1. The far-IR/submillimeter SED $\gtrsim 50$ μm is not changed by varying the inner temperature or central blackbody SED and likewise the derived temperature profile is not changed significantly at scales larger than $\sim$100 AU. Also the derived density profile at a given radius is unchanged. However, as the plot illustrates, the mid-infrared observations place good constraints on the presence of warm dust and on the spectrum of the central source. If this is assumed to be a blackbody, its temperature is constrained to be 500–1000 K. Also the fits show that the B5-IRS1 envelope cannot be warmer than 110 ± 25 K, which corresponds to inner radii of 10–40 AU. This is naturally interesting since such a constraint will limit the presence of hot gas where molecules such as H_2CO and CH_3OH can evaporate (Schöier et al. 2002, 2004a; Maret et al. 2004a; Jørgensen et al. 2004e). However, a word of caution is in place here: the exact interpretation of the mid-IR observations relies heavily on the assumed dust properties. In particular, changes in the dust opacities, e.g., when the ice mantles evaporate, will change the constraints on the source structure in the innermost region. It is therefore important to have complementary data, e.g., through imaging the chemistry and cold dust at high spatial (subarcsecond) resolution.

L1014-IRS

The second example is the L1014 core. As mentioned above, L1014 was previously assumed to be a starless core due to its lack of an IRAS 100μm source.

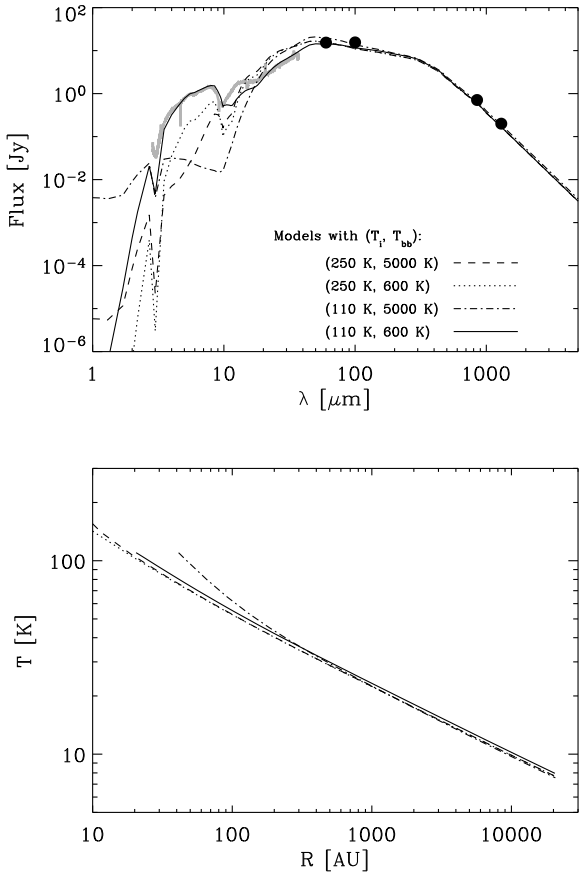

Figure 10.1. *SEDs (upper panel) and temperature profiles (lower panel) for four different models for the B5-IRS1 envelope as indicated in the left panel. In the upper panel the symbols indicate the flux measurements at far-infrared through millimeter wavelengths and the grey solid line the observations from the combined Spitzer IRS and ground-based Keck/NIRSPEC measurements.*

Its submillimeter emission is well-fitted by a Bonnor-Ebert sphere, as typically found for pre-stellar cores (e.g., Evans et al. 2001), with the interstellar radiation field (ISRF) contributing most of the luminosity. Power-law density profiles with $n \propto r^{-p}$ with $p = 1.5 - 2$, such as typically seen for protostellar envelopes, are too steep to fit the observed brightness distribution. The mass in this envelope is 1.7 $M_\odot$ with a central density of 1.5×10^5cm^{-3} at 50 AU and an outer radius of 15,000 AU. The mid-infrared imaging of Spitzer clearly reveals an infrared source toward the center of the submillimeter core with

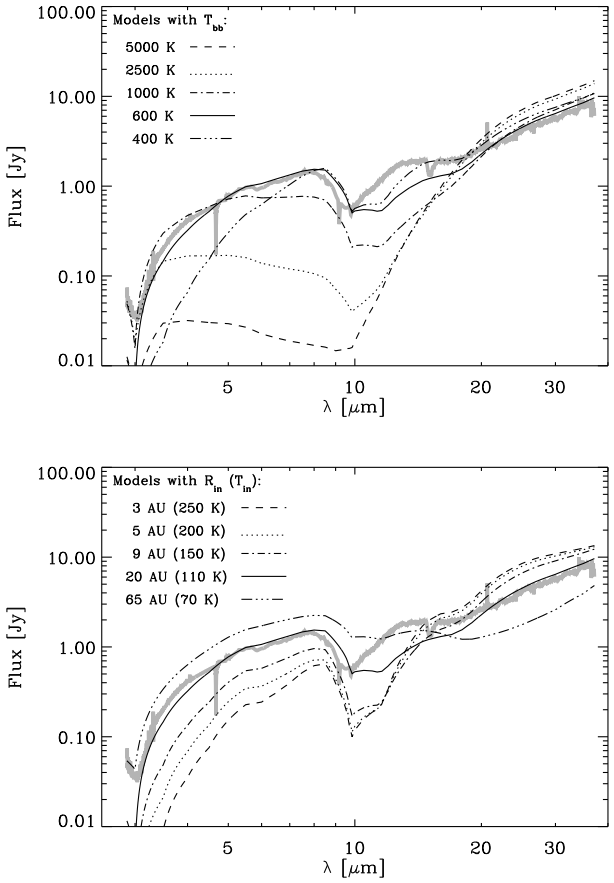

Figure 10.2. *Comparison between models with varying temperature of the central blackbody (upper panel) and envelope inner radius (lower panel). As in Fig. 10.1 the grey line inddicate the combined Spitzer and Keck measurements.*

fluxes from 4 mJy at 3.6 μm to 400 mJy at 70 μm. Although the ISRF still dominates the overall flux of the source, the IRAC (3.5–8.0 μm) fluxes can be fitted including a source with an effective temperature of 500–1000 K as illustrated in Fig. 10.3. Such a model, however, underestimates the observed MIPS (24 and 70 μm) fluxes and a cold component, possibly a circumstellar disk has to be included to account for these points. In this model the luminosity of this central "star + disk" system is very low, $\approx 0.1 L_{\odot}$, which indicates that either L1014-IRS is a very low-mass protostar (possibly a proto-brown dwarf) or that accretion is proceeding much slower than assumed within standard models.

Line observations of L1014, however, complicate this picture: CO line ob-

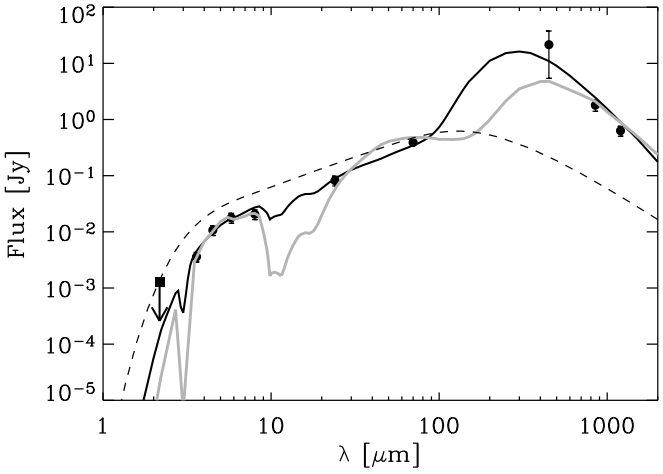

Figure 10.3. *Models for the spectral energy distribution of L1014-IRS. The black line indicates the SED of a low luminosity YSO at 200 pc, and the grey line the SED of a 16 $L_\odot$ protostar behind a 10 magnitude A_V cloud. The dashed line is the spectrum of the star+disk system for the nearby low-luminosity source. The black dots indicate the observational data from Young et al. (2004).*

servations do not reveal an outflow from the central source and do not show any condensation toward the infrared source. In fact the CO spectrum shows two components: one associated with a foreground cloud and one more distant, which may possibly be associated with the H II region, S124, at 2.6 kpc (Brand & Blitz 1993). Since HCN and CS line emission is found in the nearby component but is absent in the background cloud and since the infrared source falls within 5–10″ of the centroids of the (sub)millimeter maps, the most plausible explanation is still that L1014-IRS is associated with the foreground cloud. However, the possibility of having a protostar associated with the background cloud obscured by material at 200 pc from L1014 is a caveat which cannot be completely excluded. The two competing scenarios are sketched in Fig. 10.4

To test these possibilities a background "standard" protostar of 16 $L_\odot$ with an $n \propto r^{-1.5}$ envelope of mass 0.6 $M_\odot$ was placed behind a foreground cloud. This was simulated in two steps in DUSTY: first the SED of the background protostar was calculated as in Jørgensen et al. (2002) and thereafter the resulting spectrum was used to illuminate a 10 K planar slab with a thickness corresponding to an $A_V = 10$ cloud. The resulting SED of the protostar "in front of" and "behind" the cloud is shown in Fig. 10.5. As can be seen, the foreground cloud attenuates the mid-infrared emission and adds to the submillimeter emission thereby providing a good fit to the full observed SED. As illustrated in Fig. 10.3 it is therefore difficult to distinguish this scenario from

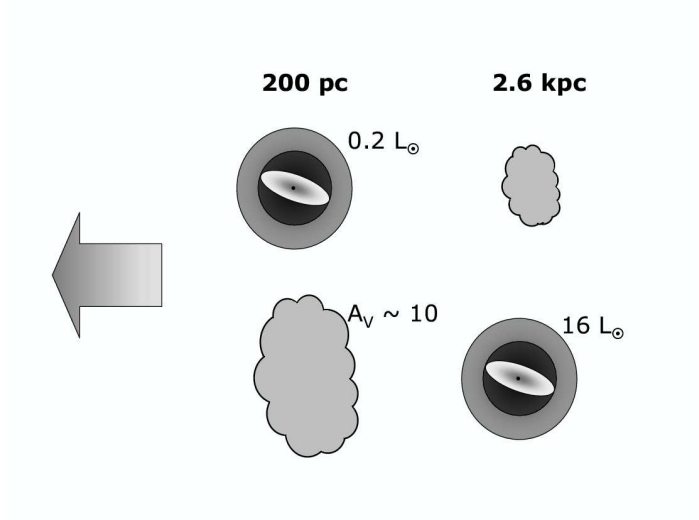

Figure 10.4. *The two scenarios for L1014. Top: a very low luminosity protostar (internal luminosity of the star+disk system of* $\sim 0.1 L_\odot$*); bottom: a background "typical"* $16 L_\odot$ *protostar behind an* $A_\mathrm{V} = 10$ *cloud.*

the nearby, low luminosity (substellar?) protostar. Complementary observations, e.g., deep searches for compact (sub)millimeter continuum emission associated with the protostar, modeling of line emission or further observations of the full 10–20 μm SED, may shed further light on this issue. This example illustrates a problem, however, which may apply to a significant fraction of the protostellar sources: they are likely embedded in larger scale clouds unaccounted for in the simple power-law density envelopes and this may affect their observable characteristics significantly.

HH46-IRS

Another complication is illustrated in the modeling of the HH46-IRS protostellar source. Again, the submillimeter and far-infrared emission constrain the single power-law density profile envelope well, especially since the peak of its spectral energy distribution is well-covered by the ISO-LWS observations. However, as shown in Fig. 10.6 the SED shortwards of 40 μm is underproduced by the envelope model. It is, however, not sufficient to change the temperature of the central black body since the column density or mass of the cold dust constrained from the far-infrared/submillimeter data makes the envelope optically thick shortwards of 40 μm. Similar experiments as for L1014, e.g., placing the source behind a foreground cloud, do not change the interpretation. The emission in such a foreground layer still makes the line of sight toward the infrared source optically thick in order to reproduce the submillimeter peak.

A more likely alternative is that the single power-law density profile breaks

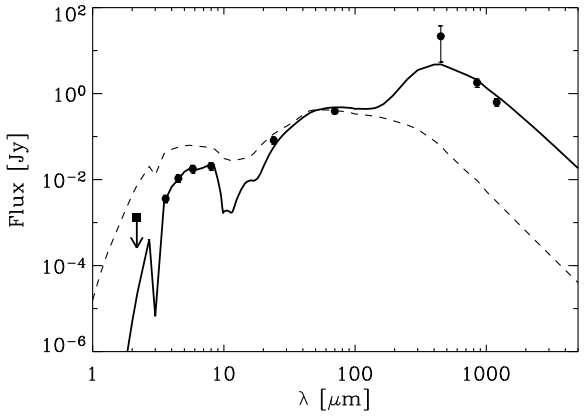

Figure 10.5. *Models for the spectral energy distribution of L1014-IRS assuming it to be a 16 $L_\odot$ background protostar. The dashed line indicates the SED of the central source with no foreground material while the solid line the SED of the source "behind" a cloud of an $A_V = 10$.*

down as a description of HH46-IRS: A flattened density profile toward the center could reduce the opacity, thereby allowing more emission from the central system to escape in the mid-IR without changing the total dust mass probed by the submillimeter emission significantly. Likewise, in a 2D model, a flattened envelope could provide the required emission at submillimeter wavelengths but still have an optically thin line of sight toward the source center at $\sim 10\mu$m. Recently Whitney et al. (2003) presented detailed 2D models for embedded protostars including circumstellar disks and outflow cavities of varying opening angles. They indeed found that different viewing angles could particularly affect the near- and mid-infrared SEDs of embedded protostars. HH46 may thus be a good candidate for studies of such non-spherical envelopes.

10.4 Applications

A number of interesting applications come from the fitting of the mid-infrared data: first the properties of the innermost region of the envelope can be directly constrained, down to where the emission becomes optically thick. This naturally feeds back to the discussion about the presence and properties of circumstellar disks as discussed in Jørgensen et al. (2004b) and Schöier et al. (2004a) and whether inner "hot regions" are present in general in protostellar envelopes as discussed by Maret et al. (2004a) and Jørgensen et al. (2004e).

The properties of the circumstellar disks are also directly hinted at from the required temperature of the central blackbody for the models: for the three sources discussed in this chapter it appears to be a robust result that a low bolo-

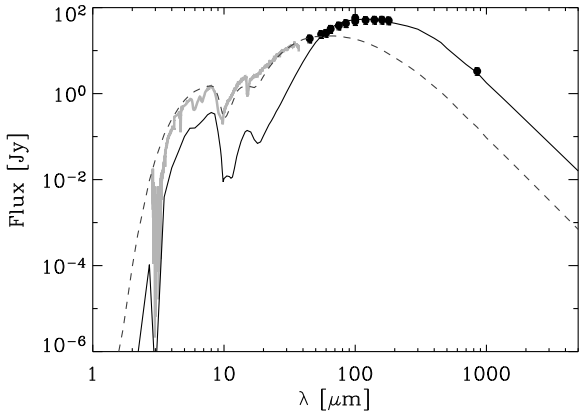

Figure 10.6. *Model for the HH46 envelope (black lines) compared to the mid-infrared Spitzer and VLT observations (grey line) and ISO-LWS and JCMT/SCUBA observations (black dots). The solid line indicates a good fit to the submillimeter/far-infrared SED, whereas the dashed line indicates the best fit to the mid-infrared SED. Both envelope models have a power-law slope of 1.5 with the first model having inner and outer radii of 400 and 30,000 AU, respectively, with a density at 1000 AU of 2×10^6 cm^{-3} whereas the latter has inner and outer radii of 80 and 2000 AU and a density at 1000 AU of 2×10^5 cm^{-3}. The latter was calculated assuming OH2 dust, i.e., dust without ice-mantles, which reproduces the 10 μm silicate feature, but does not include, e.g., the H_2O-ice at 3.1 μm.*

metric temperature of 500–1000 K is needed for the central heating source. This *does not* imply that the effective temperature of the new-formed protostellar is a blackbody of this temperature. Rather this indicates that the central source of luminosity is affected by both the SED of the newly formed star *and* of a central "cold" component, e.g., an active disk accreting material from the surrounding envelope, which, combined with the emission from the newly formed star, provide an SED peaking at 500–1000 K.

Another interesting point is the ice-composition, which can be constrained through mid-infrared observations: the adopted dust opacities from Ossenkopf & Henning (1994) represent coagulated dust grains with thin ice-mantles. These dust opacities may be inaccurate by up to a factor of two, with the fitted density profiles possibly subject to similar systematic errors. The fits from Fig. 10.7 suggest that at least some limitations exist: e.g., the observed "10 μm feature" including the contributions from silicate absorption and the H_2O ice liberation mode at 11.3 μm is significantly broader than found from the simple models and the 3.1 μm H_2O ice absorption feature is significantly overestimated (see Figure 10.7).

A first simple estimate of the fraction of material with and without ice man-

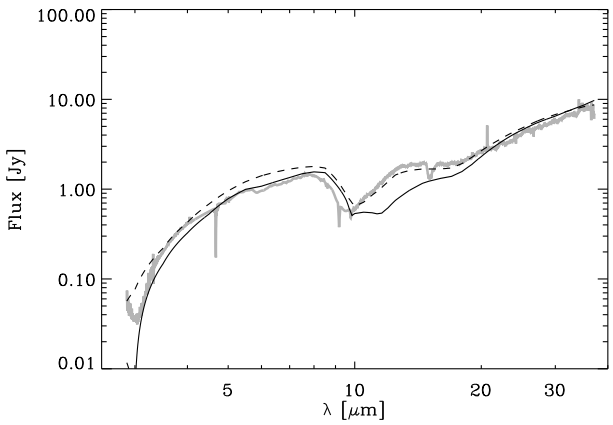

Figure 10.7. *Blow-up of the B5-IRS1 SED with the grey line the observations from Spitzer/IRS and Keck/NIRSPEC. The black solid line is the model presented in Fig. 10.1 using the "standard" dust opacities for coagulated dust grains with thin ice-mantles from Ossenkopf & Henning (1994), while the dashed line is a model for similar dust grains without ice-mantles.*

tles can be made by comparing the fractions of the column density toward the infrared source in given temperature ranges as it has been done for high-mass YSOs (see, e.g., van der Tak 2000). With knowledge of the ice optical constants (and their dependence on environment and temperature) it would be a simple task to apply the self-consistent radiative transfer models to calculate accurate synthetic spectra for different ice compositions and abundances. It would thereby be possible to establish complete molecular inventories including both gas-phase and ice species for the protostellar envelopes, which would provide an unprecedented insight into the chemistry of protostellar envelopes.

10.5 Conclusion

This chapter briefly summarizes some of the information one can hope to derive from mid-infrared observations such as obtained with the Spitzer Space Telescope or, eventually, with observations with the James Webb Space Telescope (JWST) in combination with 8 m class ground-based telescopes. The emission at mid-infrared wavelengths constrains the properties of the inner warm envelope and the spectrum of the inner source of heating, exemplified in the simple envelope models as the inner cavity and the effective temperature of the central black body. Furthermore, the self-consistent models could be applied relatively straight forwardly to also model the ice composition, e.g., by introducing different ice species and abundances at varying temperatures and radii throughout the envelope. Together with the analysis of (sub)millimeter

line observations, such results would serve as a complete inventory of both ice and gas-phase chemistry in protostellar envelopes.

A caveat is naturally to what extent the simple 1D power-law density envelopes are valid. More detailed 2D models will naturally be an important step in modeling the detailed properties of specific protostars as observational techniques become increasingly sophisticated. Still, the 1D models describe well the overall properties and appear sufficient for statistical comparisons of larger source samples. Also the most deeply embedded stages may remain elusive for detailed mid-infrared studies due to the obscuration of the central source. In any case, it is clear that the successful interpretation and complete understanding of the earliest stages of star formation relies on a wide variety of observational techniques, complementing each other. The discussions in this and the preceding chapters of this thesis are, hopefully, a step in the right direction for a more complete way of tracing the formation and physical and chemical evolution of early low-mass protostars.

Acknowledgements

Chad Young, Adwin Boogert, Klaus Pontoppidan and Kees Dullemond are thanked for interesting discussions about the early results from the Spitzer Space Telescope and their modeling. All other members of the “c2d” legacy program are thanked for all the effort in making this interesting project possible.